Synthesis, Crystal Structure, and Electrochemistry of Mono- and Bis-Homoannular Ferrocene Derivatives

Uttam R. Pokharel *, Derek Daigle , Stone Naquin , Gwyneth Engeron , Mary Lo , Frank R. Fronczek

Posted Date: 12 January 2024

doi: 10.20944/preprints202401.0965.v1

Keywords: 1,2-(α-ketotetramethylene)-ferrocene; 1,2-(tetramethylene)-ferrocene; ferrocene; Friedel-Crafts acylation; Clemmensen reduction; X-ray crystallography; planar chirality; puckering parameters; electrochemistry

Article

Synthesis, Crystal Structure, and Electrochemistry of Mono- and Bis-Homoannular Ferrocene Derivatives

Uttam R. Pokharel [1,*] Derek Daigle [1], Stone Naquin [1], Gwyneth Engeron [1], Mary Lo [1] and Frank R. Fronczek [2]

[1] Nicholls State University, Thibodaux, Louisiana 70301, USA
[2] Louisiana State University, Baton Rouge, Louisiana 70803, USA
* Correspondence: uttam.pokharel@nicholls.edu

Abstract: Two ferrocene derivatives, namely, 1,2-(tetramethylene)-ferrocene and 1,2,1′,2′-bis(tetramethylene)-ferrocene, were synthesized in a four-step reaction sequence starting from ferrocene. Friedel-Craft acylation of ferrocene with succinic anhydride gave mono- or bis(3-carboxypropinoyl)ferrocene depending on the stoichiometry of succinic anhydride. The reduction of the keto groups to methylene, followed by ring-closing using trifluoroacetic anhydride gave 1,2-(α-ketotetramethylene)-ferrocene or 1,2,1′,2′-bis(α-ketotetramethylene)ferrocene. The diastereomeric mixture of the later diketones was separated by column chromatography, characterized by single-crystal X-ray analysis, and assigned their stereochemistry. Reduction of the keto groups to methylene under Clemmensen conditions gave homoannular mono- or bis(tetramethylene) ferrocene derivatives. The molecular structure of 1,2-(tetramethylene)-ferrocene reveals that ipso carbons of the cyclopentadienyl group are 0.023(3) Å farther away from Fe(II) in comparison to its remaining three carbons. Both complexes exhibit lower half-wave oxidation potentials than ferrocene possibly due to the electron-releasing effects of the tetramethylene bridges.

Keywords: 1,2-(α-ketotetramethylene)-ferrocene; 1,2-(tetramethylene)-ferrocene; ferrocene; Friedel-Crafts acylation; Clemmensen reduction; X-ray crystallography; planar chirality; puckering parameters; electrochemistry

1. Introduction

Ferrocene and its derivatives play important roles in modern-day materials chemistry owing to their air stability, aromatic reactivity, reversible electrochemistry, and low toxicity [1]. After the discovery of ferrocene in 1951 [2], research was focused on the conjugation of carbocyclic rings to one or both cyclopentadienyl rings. The most straightforward method of such conjugation was the cyclization of ω-ferrocenylaliphatic acids. The ferrocenylaliphatic acids containing four or five carbon atoms on their side chain undergo electrophilic ring-closing to give homoannular ferrocene derivatives under electrophilic conditions [3]. Such ferrocene derivatives with unsymmetrically substituted cyclopentadienyl rings represented prototypes of *planar chirality* in metallocene chemistry due to the "sandwich" structure of the ferrocenyl moiety [4].

With our continuous interest in extending the π-conjugation of metallocenes [5], we synthesized 1′,2′,3′,4′,5′-pentamethylruthenocene-fused quinones from the double Friedel-Crafts acylation between metallocene-1,2-diacylchloride and organic aromatics [6]. Later, we realized that switching the functionality of two reaction partners can give such complexes in a much simpler method. Since ferrocene is an excellent nucleophile for Friedel-Crafts acylation, its reaction with succinic anhydride can eventually lead us to synthesize ferrocene-fused ring(s). These compounds can serve as the simplest possible model for extending the π-conjugation of metallocene. Further, ferrocene and its derivatives undergo reversible electrochemistry. Numerous studies have been concerned with the effects of substituents on the redox potential of the ferrocenyl moiety [7–10]. In general, electron-releasing substituents lower the oxidation potentials and electron-withdrawing substituents increase the potential in comparison to unsubstituted ferrocene [11]. In this contribution, we report the

 doi:10.20944/preprints202401.0965.v1

synthesis of 1,2-(tetramethylene)-ferrocene and 1,2,1′,2′-bis(tetramethylene)-ferrocene starting from ferrocene, their crystal structures, and their half-wave oxidation potentials.

2. Materials and Methods

2.1. General Procedures

Reactions were carried out using standard Schlenk line techniques under nitrogen unless otherwise mentioned. Solvents were used as received without further drying or purification. Ferrocene, succinic anhydride, aluminum chloride, zinc powder, mercuric chloride (Alfa Aesar), and trifluoroacetic anhydride (Oakwood Chemicals) were used as purchased. The organic phases were dried using anhydrous magnesium sulfate (Mallinckrodt). Flash chromatography was performed using 60-Å pore size, 230 x 400 mesh silica gel (Sorbent Technologies).

^{1}H and ^{13}C NMR spectra were recorded on a JEOL – 400 ESZ spectrometer at ca. 22 °C and were referenced to residual solvent peaks. Infrared spectra were recorded on Bruker Alpha-E FT-IR spectrometer with a diamond crystal ATR accessory. Melting points were taken on a Thomas-Hoover capillary melting point apparatus and were uncorrected. The oxidation potentials of the compounds were measured with BASi Epsilon – Electrochemical Workstation.

2.2. X-ray Crystallography

X-ray diffraction data were measured at T = 90 K on a Bruker Kappa Apex-II diffractometer equipped with a sealed-tube MoKα source (λ=0.71073 Å), a Triumph focusing monochromator and a CCD detector. Structures were solved using SHELXT [12] and refined using SHELXL [13]. Hydrogen atoms were visible in difference maps and were placed in idealized positions during refinement and treated as riding. The structure of **3b′** had a disorder involving partially occupied carbonyl groups at CH_2 sites. The crystal structures and refinement data are presented in Table 1.

2.3. Experimental Procedures

Synthesis of $C_{14}H_{14}FeO_3$ (1a). In a 500 mL flask, a mixture of succinic anhydride (1.83 g, 18.1 mmol) and aluminum chloride (4.20 g, 32.1 mmol) suspended in dichloroethane (80 mL) was added to the solution of ferrocene (3.02 g, 16.3 mmol) in dichloroethane (40 mL) over 45 minutes. The reaction mixture was allowed to stir for an additional 2 hours at room temperature and then poured into water (50 mL). The organic phase was collected. The product was extracted in 1.0 M NaOH (3 x 20 mL) and acidified with concentrated HCl until the pH of the solution dropped below 7. The precipitate was collected by filtration, washed with water, and dried to give **1a** (1.78 g, 38%) as an orange powder. **Melting point:** 165–166 °C (Lit. [14] 164 – 165). **^{1}H NMR (400 mHz, $CDCl_3$):** δ 2.72 – 2.76 (t, 2 H, ^{3}J = 6.8 Hz), 3.06 – 3.09 (t, 2 H, ^{3}J = 6.4 Hz), 4.23 (s, 5 H, Cp), 4.51 – 4.52 (t, 2 H, ^{3}J = 2.4 Hz), 4.80 – 4.81 (t, 2 H, ^{3}J = 2.0 Hz). **IR (ATR, cm^{-1}):** 1705 (C=O), 1657 (C=O).

Synthesis of $C_{18}H_{18}FeO_6$ (1b). In a 500 mL flask, succinic anhydride (10.8 g, 108 mmol) and anhydrous aluminum chloride (28.8 g, 216 mmol) were mixed in dichloroethane (80 mL). Ferrocene (10.0 g, 53.8 mmol) dissolved in dichloroethane (80 mL) was added dropwise into the flask using a dropping funnel. The reaction was stirred for 48 hours at room temperature and poured into ice water (100 mL). The solutions were layered, and the organic phase was collected. The aqueous phase was extracted with dichloromethane (100 mL). The product was extracted in 2 M sodium hydroxide (3 x 100 mL). The aqueous phase was acidified with conc. HCl until precipitation was completed. The precipitate was collected by filtration to give a crude product. The crude product was suspended in boiling water (100 mL) and filtered to give **1b** (14.9 g, 72%) as a dark red powder. Melting Point: 178 – 179 °C (Lit. [15] 179 °C). **^{1}H NMR (400 mHz, acetone-d_6, ppm):** δ 2.60 – 2.64 (t, 4 H, ^{3}J = 6.4 Hz), 3.02 – 3.05 (t, 4H, ^{3}J = 6 Hz), 4.62 – 4.63 (t, 4H, ^{3}J = 3.6 Hz), 4.89 – 4.90 (t, 4 H, ^{3}J = 2.4 Hz).

Synthesis of $C_{14}H_{16}FeO_2$ (2a). In a 250 mL flask, zinc (6.0 g, 91.8 mmol), mercuric chloride (0.60 g, 2.21mmol), DI water (20 mL), and concentrated HCl (0.30 mL) were mixed for five minutes by hand, then five minutes with a stir bar. The suspension was allowed to settle, the supernatant was decanted, washed with deionized water, then transferred into a 500 mL flask along with concentrated HCl (8.8 mL), toluene (20 mL), and compound **1a** (2.0 g, 7.00 mmol). The reaction was refluxed for 6 h. The reaction was cooled to room temperature and diluted with H_2O (20 mL). The product was extracted in ethyl ether (3 × 10 mL), then the organic layer was washed with H_2O (2 × 10 mL) and

 doi:10.20944/preprints202401.0965.v1

dried with anhydrous magnesium sulfate. The volatiles were removed *in vacuo*. The crude product was *triturated* with petroleum ether to give **2a** (1.03 g, 54%). Melting Point: 115 – 116 °C (Lit. [14] 115 – 116 °C). **^{1}H NMR (400 MHz, $CDCl_3$, ppm):** δ 1.80 – 1.87 (m, 4 H), 2.35 – 2.40 (m, 8 H), 3.98 – 4.09 (m, 8 H).

Synthesis of $C_{18}H_{22}FeO_4$ (2b). In a 250 mL flask, zinc (12.0 g, 184 mmol), mercuric chloride (1.20 g, 4.42mmol), DI water (20 mL), and concentrated HCl (0.60 mL) were mixed for five minutes by hand, then five minutes with a stir bar. The suspension was allowed to settle, the supernatant was decanted, washed with DI water, then transferred into a 500 mL flask along with H_2O (8 mL), concentrated HCl (17.6 mL), toluene (20 mL), and compound **1b** (4.0 g, 10.4 mmol). The reaction was refluxed for 19 hours. The reaction was cooled to room temperature and diluted with H_2O (20 mL). Unreacted zinc was separated by decantation and the residue was washed with diethyl ether (30 mL). The organic layer was collected, and the aqueous phase was extracted with diethyl ether (2 x 50 mL). The combined organic phase was dried with anhydrous magnesium sulfate. Volatiles were removed *in vacuo*. The final product was purified by *trituration* with petroleum ether to give **2b** (3.36 g, 90%) as a yellow powder. Melting Point: 72 – 73 °C (Lit. [15] 73 °C). **^{1}H NMR (400 mHz, $CDCl_3$, ppm):** δ 1.80 – 1.87 (m, 4H), 2.35 – 2.40 (m, 8H), 43.98 – 4.09 (m, 8H). **^{13}C{^{1}H} NMR (100 MHz, $CDCl_3$, ppm):** δ 25.95, 28.58, 33.64, 67.89, 68.88, 77.32, 88.08, 179.97. **IR (ATR, cm^{-1}):** 1703 (C=O), 3000 – 3200 (OH).

Synthesis of $C_{14}H_{14}FeO$ (3a). In a 100 mL flask, trifluoroacetic anhydride (0.620 mL) was mixed with dichloromethane (33 mL). A mixture of compound **2a** (1.00 g, 3.67 mmol) and dichloromethane (33 mL) was added dropwise to the flask *via* a dropping funnel and the reaction was allowed to stir for 8 hours at room temperature. A saturated solution of $NaHCO_3$ (10 mL) was added and the mixture was layered in a separatory funnel. The organic layer was collected, dried with anhydrous $MgSO_4$ and volatiles were removed *in vacuo* to give **3a** (0.758 g, 81%). Melting Point: 82 – 83 °C (Lit. [16] 83 – 85 °C) **^{1}H NMR (400 MHz, $CDCl_3$, ppm):** δ 2.02 – 2.22 (m, 2H), 2.25 – 2.45 (m, 2H), 2.59 – 2.67 (m, 2H), 4.17 (s, 5H, Cp), 4.45 – 4.47 (m, 2H, Cp), 4.81 – 4.82 (m, 1H, Cp). **^{13}C{ NMR (100 MHz, acetone-d_6, ppm):** δ 23.4, 23.9, 38.8, 64.6, 70.0, 75.8, 92.5, 202.4. **IR (ATR, cm^{-1}):** 1664 (C=O). The product was analyzed by single crystal X-ray analysis.

Synthesis of $C_{18}H_{18}FeO_2$ (3b and 3b'). In a 100 mL flask, **8** (0.501 g, 1.40 mmol) was dissolved in dichloromethane (15 mL). Trifluoroacetic anhydride (0.778 mL, 5.59 mmol) in dichloromethane (15 mL) was added dropwise. The reaction was stirred for 20 hours at room temperature. Sodium bicarbonate solution (10%, 100 mL) was added to the mixture and layered with dichloromethane. The organic layer was collected, washed with water (2 × 20 mL), dried with magnesium sulfate, and filtered. The filtrate was evaporated to dryness to give **3b** and **3b'** (0.190 g, 42%) as a bright red powder. The two diastereomers were separated by column chromatography in silica using a mixture of ethyl acetate and dichloromethane (2:1 by volume). The racemic mixture (dark red), **3b'** was followed by the *meso* (dark orange), **3b** in the column. **3b** (*Meso):* Melting Pont: 168 -189 °C (Lit. [17] 161 -167 °C. **^{1}H NMR (400 mHz, $CDCl_3$):** δ 2.00 -2.11 (m, 4H, CH2), 2.15 – 2.40 (m, 6H, CH2), 2.56 – 2.66 (m 4H CH2), 4.42 – 4.45 (m, 2H, Cp), 4.73 (b, 2H, Cp). **^{13}C{ NMR (100 MHz, $CDCl_3$, ppm):** δ 22.92, 23.66, 39.27, 67.38, 72.37, 73.19, 76.58, 93.42, 204.33. **IR (ATR, cm^{-1}):** 1661 (C=O). The product was characterized by single crystal X-ray analysis. **3b'***(Racemic):* Melting Point: 156 - 157 °C (Lit. [17] 153 – 161 °C). **^{1}H NMR (400 mHz, $CDCl_3$):** δ 2.01 – 2.15 (m, 2 H), 2.21 – 2.47 (m, 6H), 2.61 (dt, ^{2}J = 15.6 Hz, ^{3}J = 4.4 Hz, 4 H), 4.39 (d, ^{3}J = 1.2 Hz, 2H), 4.42 – 4.43 (m, 4 H), 4.65 (t, 3J = 1.2 Hz, 2 H). **^{13}C{ NMR (100 MHz, $CDCl_3$, ppm):** δ 23.32, 23.52, 39.20, 68.03, 70.84, 71.85, 77.32, 94.00, 203.40 **IR (ATR, cm^{-1}):** 1663 (C=O). The product was analyzed by single crystal X-ray analysis.

Synthesis of $C_{14}H_{16}Fe$ (4a). In a 250 mL flask, zinc (5.0 g, 76.4 mmol), mercuric chloride (0.5 g, 1.84 mmol), and DI water (20 mL) were mixed for 10 min. The suspension was allowed to settle, the supernatant was decanted, and the residue was washed with DI water. To the amalgamated zinc, concentrated HCl (2.0 mL), toluene (20 mL), and compound **3** (200 mg, 0.787 mmol). The reaction was refluxed for 2 h and an additional amount of conc. HCl (2.0 mL) was added and continued reflux for another 3 h. The reaction was cooled to room temperature, the clear solution was decanted, and the unreacted zinc was washed with ethyl acetate (40 mL). The combined organic layer was washed with water (3 x 100 mL), dried with anhydrous $MgSO_4$, and filtered. The volatiles were removed *in vacuo* to give **4a** (166 mg, 87%) as a yellow solid. Melting point: 39 °C (Lit. [18] 39 – 41 °C) **^{1}H NMR (400 MHz, Acetone-d_6, ppm):** δ 1.53 – 1.64 (m, 2H), 1.85 – 1.92 (m, 2H), 2.17 – 2.26 (m, 2H), 2.60 – 2.67 (m,

Preprints (www.preprints.org) | NOT PEER-REVIEWED | Posted: 12 January 2024 doi:10.20944/preprints202401.0965.v1

2H), 3.85 (t, ^3J = 2.4 Hz, 1H, CHC*H*CH), 3.94 (d, ^3J = 2.4 Hz, 2H, C*H*CHC*H*), 3.95 (s, 5H, Cp). **^{13}C{^{1}H}, acetone-d$_6$, ppm):** δ 23.5, 24.6, 64.8, 65.1, 69.4, 84.9.

Synthesis of $C_{18}H_{22}Fe$ (4b). In a 100 mL flask, a mixture of zinc (5.0 g, 76.47 mmol), mercuric chloride (0.50 g, 1.84 mmol), and DI water (20 mL) was stirred for 10 min. The clear solution was decanted and the residue was washed with DI water (20 mL). To the activated Zn, the diastereomeric mixture of **3b** and **3b'** (200 mg, 0.62 mmol), toluene (20 mL), and conc. HCl (2.0 mL) was added. The reaction was refluxed for 3 h and an additional amount of conc. HCl (4.0 mL) was added. The reaction was again refluxed for 2 h. The mixture was cooled to RT and the soluble product was decanted. The residue was washed with ethyl acetate (2 x 10 mL). The extract was washed with water (2 x 80 mL); the organic layer was collected, dried over anhydrous $MgSO_4$, and filtered. Volatiles were removed *in vacuo*. The crude product was purified by silica gel column chromatography using petroleum ether as eluent to give **4b** (107 mg, 59%) as yellow gum. **^{1}H NMR (400 mHz, acetone-d$_6$):** δ 1.53 – 1.57 (m, 4H), 1.85 – 1.88 (m, 4H), 2.16 – 2.23 (m, 4H), 2.57 – 2.64 (m, 4H), 3.65 (t, ^3J = 2.4 Hz, 2H, CHC*H*CH), 3.76 (d, 3J = 2.4 Hz, 4H, C*H*CHC*H*). **^{13}C{ NMR (100 MHz, acetone-d$_6$, ppm):** δ 23.6, 23.9, 67.5, 68.3, 84.2.

3. Results and discussion

3.1. Synthesis and Structural Elucidation of Compounds 1a, 1b – 4a, 4b

Synthesis of the target compounds (**4a** and **4b**) was performed by following the reaction sequence as shown in Scheme 1. Our attempts to reproduce the procedures reported in the literature [19,20] resulted in the formation of a mixture of both mono-and bis(3-carboxypropenoyl)ferrocene in a ca. 1:1 ratio. To avoid the tedious separation of these two keto-carboxylic acids, we synthesized (3-carboxypropenoyl)ferrocene, **1a** (38%) by slowly adding a suspension of succinic anhydride and aluminum chloride in dichloroethane to the solution of ferrocene in the same solvent. The procedure left some unreacted ferrocene, but the product was purified by solvent extraction using NaOH solution. Synthesis of bis(3-carboxypropenoyl)ferrocene, **1b** (72%) was performed by adding ferrocene into the suspension of succinic anhydride and aluminum chloride and stirring the solution at room temperature for 48 hours. After the base extraction, the product was found to contain **1a** as an impurity which was removed by washing it with hot water. The Clemmensen reduction of both keto carboxylic acids was performed by following the literature procedures [14,15] with slight modifications to give mono- and bis(3-carboxypropyl)ferrocene **2a** (54%) and **2b** (90%), respectively.

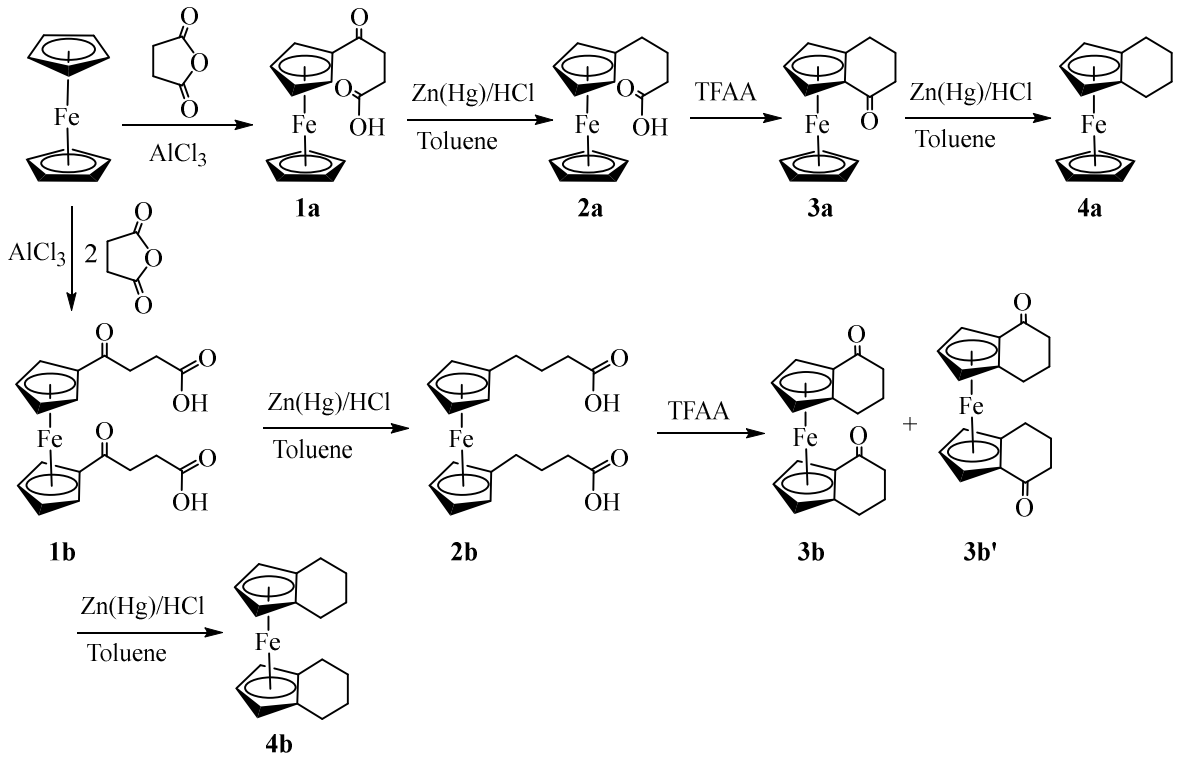

 doi:10.20944/preprints202401.0965.v1

Scheme 1. Synthesis of homoannular ferrocene derivatives.

The ring closing of **2a** and **2b** was performed in the presence of trifluoroacetic anhydride [17,21] to give homoannularly cyclized products: 1,2(α-ketotetramethylene)ferrocene, **3a** (81%) and 1,2,1′,2′-bis(α-ketotetramethylene)ferrocene, **3b** (42%) respectively. Although Nesmeyanov[22] and Rinehart [3,17] independently reported the synthesis of **3a** and **3b**, their full characterization data were not available. The diketone **3b** must exist as two geometric isomers (*racemic* and *meso*) but the authors were unable to assign the configurations of the diastereomers [17]. Based on ^{1}H NMR analysis of the crude product, we observed the formation of these isomers in ca. 1:1 ratio. Assignment of the stereochemistry of these geometrical isomers (**3b** and **3b′**) was performed by single crystal X-ray analysis (*vide infra*). The ^{1}H NMR of **3a, 3b** and **3b′** exhibited a distinctive ABC pattern of substituted cyclopentadienyl rings. Similarly, the diastereotopic nature of *exo*- and *endo*-protons of the methylene groups exhibited a complex coupling pattern giving a set of multiplets.

The keto groups of **3a, 3b,** and **3b′** were reduced to methylene under Clemmensen conditions to give 1,2-(tetramethylene)-ferrocene **4a** (87%) and 1,2,1′,2′-bis(tetramethylene)-ferrocene **4b** (59%), respectively. The loss of carbonyl stretching in IR and the appearance of triplets (1H) and doublets (2H) on the substituted cyclopentadienyl rings in ^{1}H NMR indicated the formation of desired products. Like ketones (**3a**, **3b,** and **3b′**), the diastereotopic nature of the *exo*- and *endo*-hydrogens of the methylene group gave a complicated coupling pattern. Compound **4b** exhibited four sets of CH_2 protons and two sets of cyclopentadienyl protons indicating the free rotation of two Cp rings with respect to the Fe(II) center. Moreover, both signals of cyclopentadienyl rings are shifted upfield for both **4a** and **4b** but the shift is more prominent for **4b** (triplet at 3.65 and doublet at 3.75 ppm). Compounds **4a** and **4b** were previously synthesized by the catalytic hydration of (cyclopentadienyl)(indenyl)iron [18] or bis(indenyl)iron [23]. Synthesis of **4b** was also reported from the condensation of spiro[4·4]nona-1,3-diene with iron[24] as well as the treatment of the lithium salt of 4,5,6,7-tetrahydroindene with $FeCl_2$ [25].

3.2. X-ray Crystal Structures

The structures of ferrocene derivatives **3a**, **3b**, **3b′,** and **4a** were determined by X-ray crystallographic methods. All crystals were grown by slow evaporation of concentrated ethyl ether solution in air at room temperature. Thermal ellipsoid plots with numbering schemes are shown in Figures 1–4. The crystal structure and refinement data for these compounds are given in Table 1. The crystal structure of **3a** has been reported by Fleischer, et al. at room temperature [26]. We have redetermined its crystal structure at 90 K with a much higher precision level. The compound **3a** exhibits planar chirality since two different substituents are connected to the cyclopentadienyl ring [27]. As the compound crystallizes in centrosymmetric space group (*P*−1), the two enantiomers *R*p/*S*p are present in equal numbers within the crystals. The iron atom in compound **3b** lies on a crystallographic inversion center. Compound **3b′** crystallizes with Z′ = 2 in which one of the molecules has a disorder of O atom in two positions. The **3b′** crystallizes as a racemic mixture in a centrosymmetric space group $P2_1/n$. The two molecules have a roughly perpendicular orientation. Each molecule possesses an approximate crystallographic two-fold rotational axis (Figure 3). Compound **4a** crystallizes in the *monoclinic* space group $P2_1/c$ with one molecule per asymmetric unit.

Preprints (www.preprints.org) | NOT PEER-REVIEWED | Posted: 12 January 2024 doi:10.20944/preprints202401.0965.v1

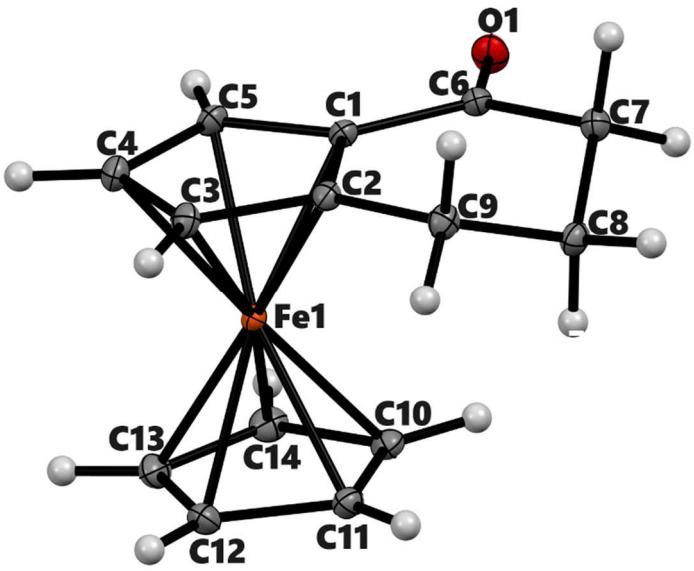

Figure 1. ORTEP diagram of solid-state structure showing the atom-numbering scheme of compound **3a.** Thermal ellipsoids are drawn at the 50% probability level. Selected bond lengths (Å) for the complex: Fe1–C1 2.0397(9), Fe1–C2 2.0508(8), Fe1–C3 2.0526(6), Fe1–C4 2.0527(7), Fe1–C5 2.0456(9), Fe1–C10 2.0553(7), Fe1–C11 2.0530(8), Fe1–C12 2.045(1), Fe1–C13 2.0548(9), Fe1–C14 2.0554(6), C1–C6 1.465(1), C6–O1 1.2265(9), Cp (centroid, substituted) – Fe 1.647, Cp (centroid, unsubstituted) 1.655.

In the molecules of **3a**, **3b,** and **3b'** the ferrocenyl moiety is fused with α-keto tetramethylene rings with one of both cyclopentadienyl rings while in the molecules of **4a**, the ferrocenyl moiety is fused with tetramethylene ring. In all molecules, the angle between Fe and two Cp ring centroids is nearly 180° with a maximum deviation of 4.85° from linear geometry in **3b'**. The Cp rings in the ferrocene system are almost parallel; as the dihedral angle between the planes of two Cp rings in **3a**, **3b',** and **4a** are 1.84°, 3.46° (average of two), and 1.92°, respectively. The Cp rings display nearly eclipsed conformation on **3a**, **3b'**and **4a**, as demonstrated by C – Cg1 – Cg2 – C average torsion angles of 9.12°, 0.26°, and 6.12° respectively. The Cp rings in **3b** are in perfectly staggered conformation (torsional angle 36.00°) as required by the inversion center located at Fe.

Preprints (www.preprints.org) | NOT PEER-REVIEWED | Posted: 12 January 2024 doi:10.20944/preprints202401.0965.v1

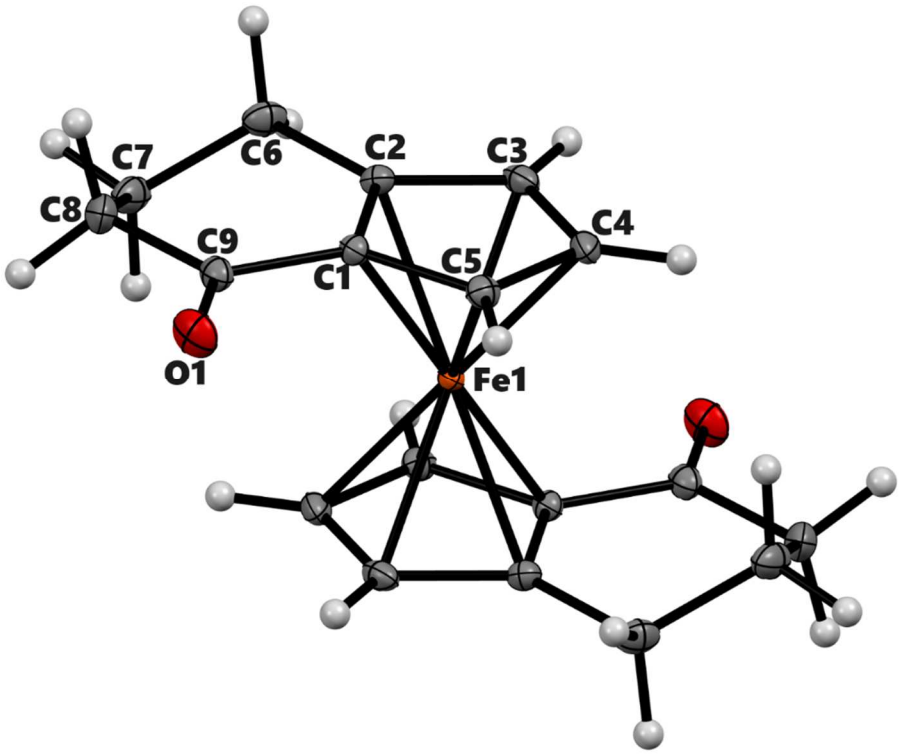

Figure 2. ORTEP diagram of the solid-state structure showing the atom-numbering scheme of compound **3b** (*meso*). Thermal ellipsoids are drawn at the 50% probability level. Selected bond lengths (Å) for the complex: Fe1–C1 2.0397(8), Fe1–C2 2.0627(7), Fe1–C3 2.0605(8), Fe1–C4 2.0664(8), Fe1–C5 2.0511(7), O1–C9 1.2230(9), Cp (centroid)–Fe 1.660.

Within the ferrocenyl moieties, the mean Fe – C bond distances for unsubstituted Cp are unremarkable. However, the Fe–C distance for the *ipso* carbon-bearing keto group next to it is slightly shorter than the rest of the distances. For instance, Fe1 – C1 bond in compound **3a** is 2.0397(9) Å while the average distance of Fe1 with C2 to C5 is 2.0505(7) Å. The slippage of the Fe center towards C1 has been observed in other α-keto ferrocenyl derivatives [28,29]. The slipping of Fe1 towards C1 presumably occurs to maximize the interaction of the Fe center with the exocyclic double bond in the resonance of such ketones [30]. The attached carbonyl group lies almost co-planar with the plane of the substituted cyclopentadienyl ring in **3a 3b** and **3b′** as given by the torsional angle [C5-C1-C6-O1 = 1.52(11)°] in **3a**. The C=O bond length in **3a** 1.2265(9) Å, **3b** 1.2230(9) Å, and **3b′** 1.225 (17) Å are in normal range of similar α-ferrocenyl ketones.[31,32] In **4a**, the average of Fe1-C1 and Fe1-C2 distances is higher by 0.023(3) Å than the rest of Fe-C bonds of the substituted cyclopentadienyl ring. The distance of the Fe center from the centroid of cyclopentadienyl rings ranges from 1.647 Å to 1.660 Å.

Preprints (www.preprints.org) | NOT PEER-REVIEWED | Posted: 12 January 2024 doi:10.20944/preprints202401.0965.v1

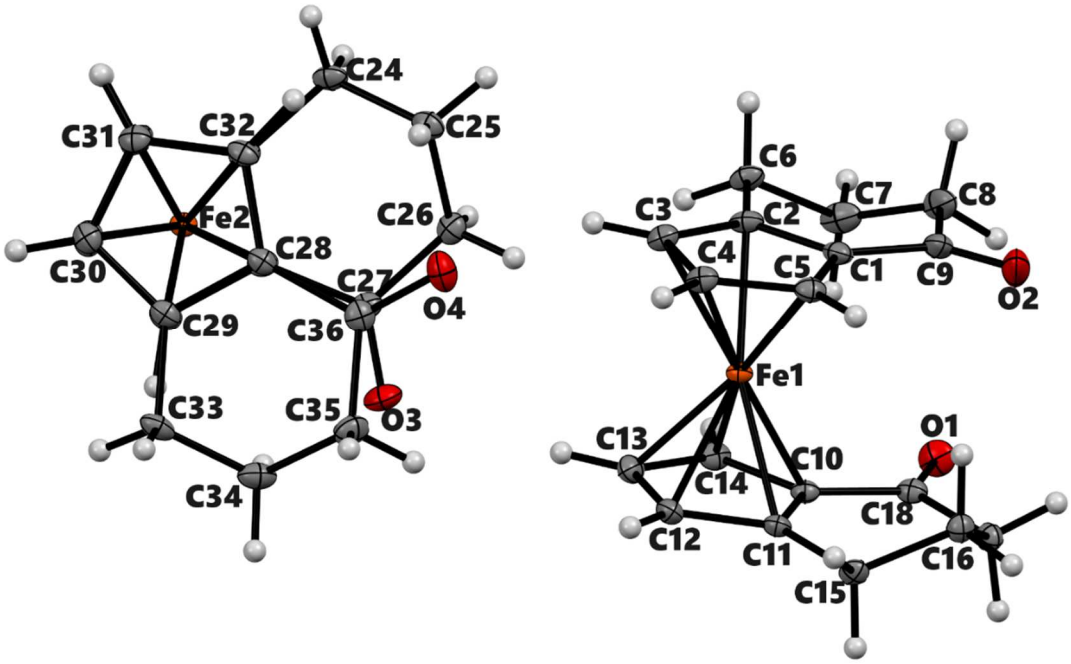

Figure 3. ORTEP diagram of the solid-state structure showing the atom-numbering scheme of compound **3b'**. Thermal ellipsoids are drawn at the 50% probability level. The minor component of disordered O-atom is not shown. Selected bond lengths (Å) for the complexes: Fe1–C1 2.0409(7), Fe1–C2 2.0575(7), Fe1–C3 2.0681(7), Fe1–C4 2.0534(7), Fe1–C5 2.0442(7), Fe1–C10 2.0469(6), Fe1–C11 2.0688(6), Fe1–C12 2.0615(7), Fe1–C13 2.0566(7), Fe1–C4 2.0534(7), Fe1–C4 2.0534(7), O2–C9 1.2212(17), Average Cp(Centroid)–Fe 1.652.

The six-membered rings in all structures adopt half-chair conformations. The Cremer & People puckering parameters [33] of the six-membered rings, namely, 3a, 3b, 3b′ and 4a are Q_T = 0.4340(8) Å, θ = 131.43(11)° and φ = 2.47(14)°; Q_T =0.4227(8) Å, θ = 129.68(10)° and φ = 358.42(13)°; Q_T = 0.4356(12) Å, θ = 53.54(14)° and φ = 178.20(18)°; and Q_T = 0.521(3) Å, θ = 51.7(3)° and φ = 219.0(4)°, respectively. In **3a,** atoms C6/C7/C9 lie on the same plane of the substituted cyclopentadienyl ring with a dihedral angle of 1.80°. The C8 projects inward from the main plain of Cp by 0.582 Å. Similar folding of six-membered rings can be seen in **3b** and **3b'** as well. The two α-ketotetramethylene groups are oriented with dihedral angles of 180° and 72° in **3b** and **3b'**, respectively. The six-membered ring of **4a** is more twisted than in **3a** or **3b**. In this molecule, **C6** and **C9** are almost coplanar with the substituted Cp [deviation: C6 = 0.018 Å, C9 = 0.033 Å]. The C7 is projected down by 0.498 Å and C8 is projected up by 0.305 Å from the Cp plane.

Preprints (www.preprints.org) | NOT PEER-REVIEWED | Posted: 12 January 2024 doi:10.20944/preprints202401.0965.v1

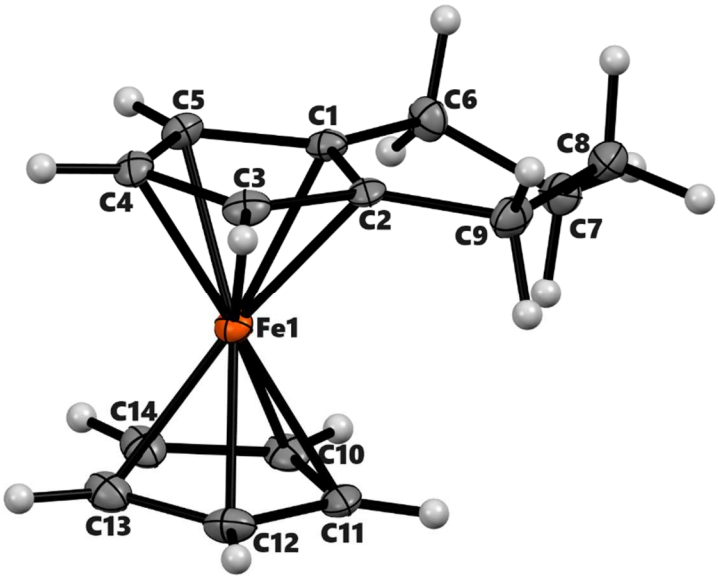

Figure 4. ORTEP diagram of solid-state structure showing atom-numbering scheme of compound **4a**. Thermal ellipsoids are drawn at the 50% probability level. Selected bond lengths (Å) for the complexes: Fe1–C1 2.049(3), Fe1–C2 2.064(3), Fe1–C3 2.040(3), Fe1–C4 2.034(2), Fe1–C5 2.031(3), Fe1–C10 2.043(3), Fe1–C11 2.036(3), Fe1–C12 2.045(3), Fe1–C13 2.051(3), Fe1–C14 2.042(3), Cp (centroid, substituted) – Fe 1.647, Cp (centroid, unsubstituted) 1.648.

Table 1. Crystal data and refinement.

	3a	**3b** *(meso)*	**3b'** *(racemic)*	**4a**
Chemical formula	$C_{14}H_{14}FeO$	$C_{18}H_{18}FeO_2$	$C_{18}H_{18}FeO_2$	$C_{14}H_{16}Fe$
M_r	254.1	322.17	322.17	240.12
Deposition No.	CCDC 2322201	CCDC 2322202	CCDC 2322203	CCDC 2322204
Crystal system, space group	Triclinic, *P*-1	Monoclinic, $P2_1/n$	Monoclinic, $P2_1/n$	Monoclinic, $P2_1/c$
Temperature (K)	90	90	90	90
a, *b*, *c* (Å)	6.5983 (4), 7.7105 (4), 11.8843 (7)	7.422 (2), 7.551 (2), 12.366 (4)	13.6414 (6), 14.7516 (6), 13.8763 (6)	7.661 (3), 9.506 (4), 14.642 (6)
α, β, γ (°)	108.140 (3), 90.461 (3), 108.897 (3)	90, 100.397 (14), 90	90, 99.432 (2), 90	90, 95.574 (6), 90
V (Å^3)	539.61 (6)	681.6 (3)	2754.6 (2)	1061.4 (7)
Z	2	2	8	4
Radiation type	Mo *Kα*	Mo *Kα*	Mo *Kα*	Mo *Kα*
μ (mm^{-1})	1.37	1.11	1.10	1.38
Crystal size (mm)	0.16 × 0.15 × 0.06	0.36 × 0.20 × 0.11	0.44 × 0.39 × 0.36	0.15 × 0.11 × 0.06
Diffractometer	Bruker Kappa *APEX*-II DUO	Bruker Kappa *APEX*-II	Bruker Kappa *APEX*-II DUO	Bruker Kappa *APEX*-II DUO
Absorption correction	Multi-scan	Multi-scan	Multi-scan	Multi-scan
T_{min}, T_{max}	0.863, 0.922	0.750, 0.888	0.657, 0.749	0.753, 0.922

Preprints (www.preprints.org) | NOT PEER-REVIEWED | Posted: 12 January 2024 doi:10.20944/preprints202401.0965.v1

No. of measured, independent and observed [$I > 2\sigma(I)$] reflections	22162, 9304, 7739	22653, 5593, 4567	74998, 21250, 16339	16912, 3242, 1949
R_{int}	0.025	0.026	0.028	0.139
$(\sin\theta/\lambda)_{max}$ (Å^{-1})	1.042	1.018	0.974	0.716
$R[F^2 > 2\sigma(F^2)]$, $wR(F^2)$, S	0.034, 0.081, 1.04	0.030, 0.084, 1.07	0.033, 0.090, 1.05	0.052, 0.100, 1.00
No. of reflections	9304	5593	21250	3242
No. of parameters	187	97	400	136
No. of restraints	0	0	9	0
H-atom treatment	Only H-atom coordinates refined	H-atom parameters constrained	H-atom parameters constrained	H-atom parameters constrained
$\Delta\rho_{max}$, $\Delta\rho_{min}$ (e Å^{-3})	1.38, −0.75	1.05, −0.77	1.47, −0.53	0.66, −0.85

In their crystal structures, compounds **3a**, **3b,** and **3b'** display similar intermolecular interactions. In these molecules, the most prominent interactions are weak intermolecular C-H···O hydrogen bonds and C-H···π interactions. For example, molecules of **3b** exhibit intermolecular C4-H4···O1, C-H5···O1 interactions along the crystallographic *b*-axis. Similarly, atom H8A is positioned almost perpendicular above the cyclopentadienyl ring centroid of the adjacent molecule (Figure 5 (I). In the crystal structure of **4a**, there are C-H···π interactions between methylene hydrogen and the cyclopentadienyl rings (Figure 5 (II)).

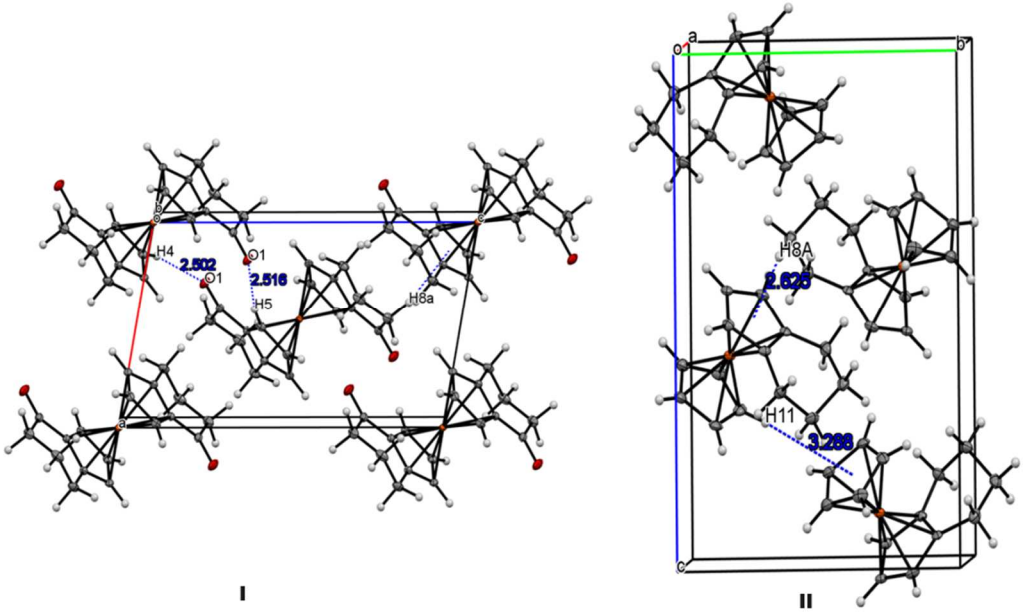

Figure 5. (I) Packing diagram of **3b** along the *b* axis; (II) packing of **4a** along *a* axis (II).

3.3. Electrochemical studies

To investigate the effects of tetramethylene substituents on the oxidation potential of the ferrocene moiety, we measured the half-wave redox potentials ($E_{1/2}$) of **4a** and **4b** by cyclic voltammetry using 0.1 M tetrabutylammonium hexafluorophosphate in dichloromethane as a

Preprints (www.preprints.org) | NOT PEER-REVIEWED | Posted: 12 January 2024 doi:10.20944/preprints202401.0965.v1

supporting electrolyte at a scan rate of 50 mV s^{-1} in 10^{-3} M concentration. All measurements were carried out at room temperature under a dry nitrogen atmosphere by the use of a three electrode system: glassy carbon as the working electrode, Ag/AgCl as the reference electrode, and platinum wire as a counter electrode.

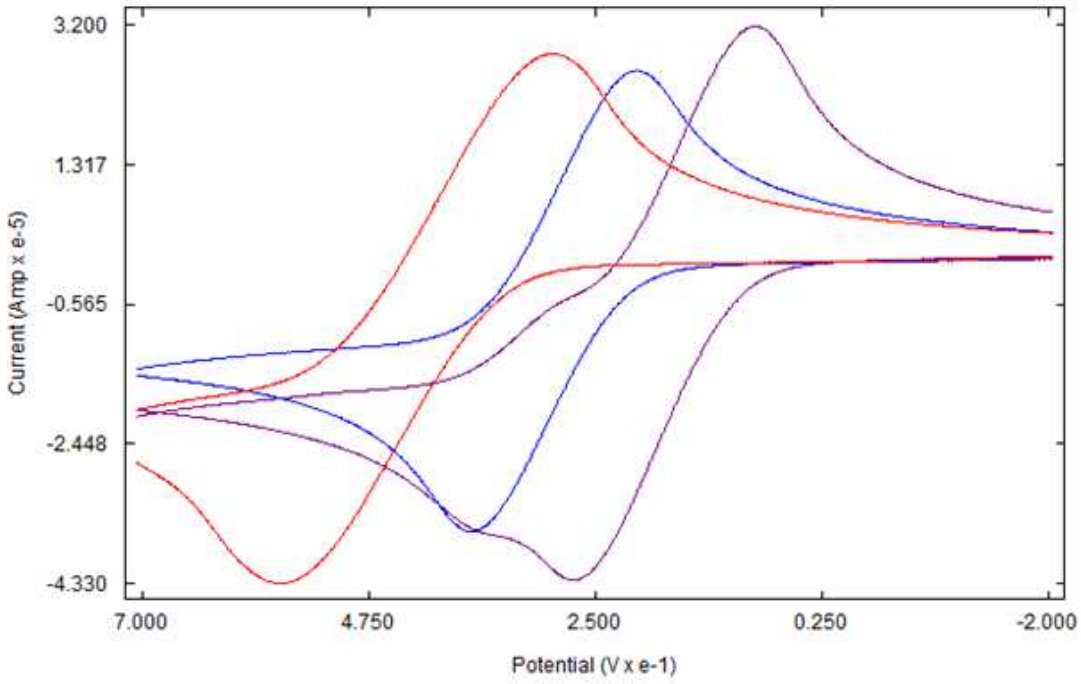

Figure 5. Cyclic voltammogram of Ferrocene (red), **4a** (blue), and **4b** (purple).

Like ferrocene, the cyclic voltammetry of **4a** and **4b** shows a single-electron reversible redox process (Figure 5). As expected, the redox potentials of both complexes were lower than that of ferrocene due to the electron-releasing ability of tetramethylene rings. The higher electron density at the iron center due to the tetramethylene ring causes the iron center to lose an electron more easily in comparison to ferrocene [34]. Figure 6 shows a plot of $E_{1/2}$ *vs.* the number of tetramethylene groups. Under the experimental conditions, the $E_{1/2}$ of ferrocene, **4a** and **4b** are 499 mV, 303 mV, and 183 mV, respectively *versus* Ag/Ag^{+}. Although there is a sharp decrease in the potential, the relationship between the number of substituents and oxidation potential is not linear. The difference in potential between ferrocene and **4a** is 196 mV, while the difference between **4a** and **4b** is just 120 mV. The number of tetramethylene bridges in **4b** is double that of **4a**. However, the expected decrease in potential is less than half. A slightly higher potential of **4b** than its predicted value might be due to the steric bulk of additional tetramethylene rings around the iron center that render the interaction of the iron atom with the electrode difficult [35].

Preprints (www.preprints.org) | NOT PEER-REVIEWED | Posted: 12 January 2024 doi:10.20944/preprints202401.0965.v1

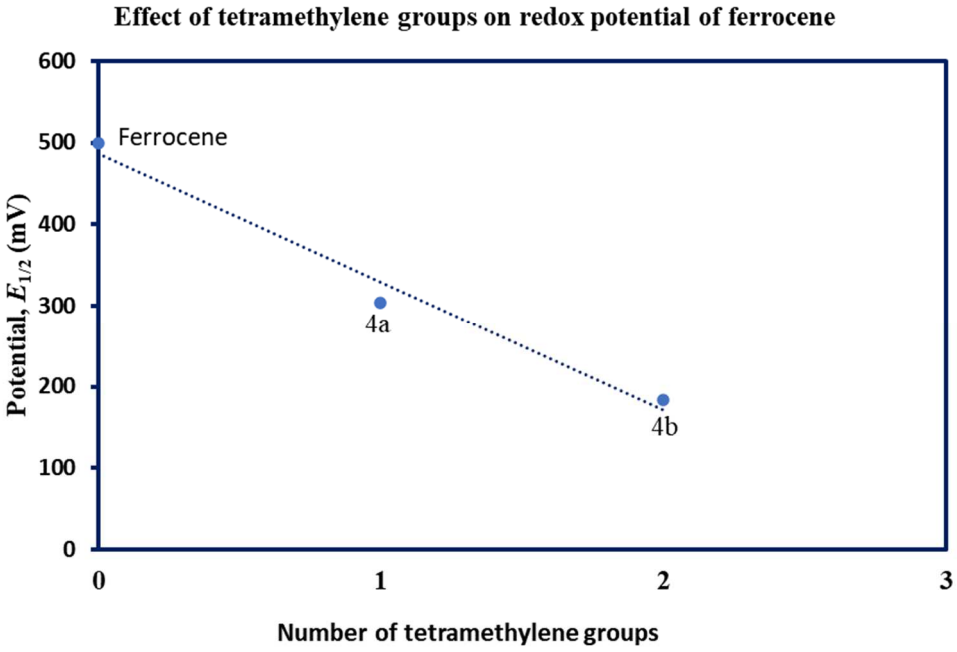

Figure 6. Effects of substituents in the redox potential of ferrocene derivatives.

4. Conclusions

We have synthesized and characterized mono- and bis-tetramethyleneferrocenes as viable precursors of π-extended ferrocene derivatives. Four compounds of the reaction sequence have been studied with single-crystal X-ray analysis. The effects of tetramethylene groups on the half-wave oxidation potential have been studied by cyclic voltammetry. Our attempts to dehydrogenate the final products of this reaction sequence with 2,3-Dichloro-5,6-dicyano-1,4-benzoquinone (DDQ) were unsuccessful. Currently, we are working on alternative methods to aromatize the ferrocene-bound aliphatic rings.

Supplementary Materials: The following supporting information can be downloaded at the website of this paper posted on Preprints.org, Figure S1: 1H NMR of 3a; Figure S2: 13C NMR of 3a; Figure S3: 1H NMR of 3b; Figure S4: 13C NMR of 3b; Figure S5: 1H NMR of 3b'; Figure S6: 13C NMR of 3b'; Figure S7: 1H NMR of 4a; Figure S8: 13C NMR of 4a; Figure S9: 1H NMR of 4b.

Author Contributions: Conceptualization, U. P. synthesis, and spectroscopic characterization, D. D., S. N., G. E. X-ray crystallography, F. F. electrochemistry, M. L., U. P. writing – original draft preparation, U. P. writing – review and editing, U. P. and F. F. visualization, U. P. supervision, U. P. project administration, U. P. funding acquisition, U. P.

Funding: The work was funded by the Louisiana Board of Regents. Contract number: LEOSF (2017-18)-RD-A-28.

Data Availability Statement: Data are contained within the article and Supplementary materials.

Acknowledgments: The authors extend their appreciation to the Department of Chemistry and Physical Sciences, Nicholls State University for providing funds for purchasing chemicals, and the Department of Chemistry, Louisiana State University for providing X-ray crystallography services free of charge.

Conflicts of Interest: The authors declare no conflict of interest.

References

1. Astruc, D. Why is ferrocene so exceptional? European Journal of Inorganic Chemistry 2017, 2017, 6-29, doi:org/10.1002/ejic.201600983.
2. Kealy, T.J.; Pauson, P.L. A New Type of Organo-Iron Compound. Nature 1951, 168, 1039-1040, doi:10.1038/1681039b0.
3. Rinehart, K.L., Jr.; Curby, R.J., Jr. Ferrocene bridging and homoannular cyclizations. Journal of the American Chemical Society 1957, 79, 3290-3291, doi:10.1021/ja01569a084.

4. Schlögl, K. Stereochemistry of metallocenes. Topics in stereochemistry 1967, 39-91, doi:org/10.1002/9780470147108.ch2.
5. Pokharel, U.R. Organometallic heterocycles and acene-quinone complexes of ruthenium, iron and manganese. PhD dissertation, University of Kentucky, 2012.
6. Pokharel, U.R.; Selegue, J.P.; Parkin, S. Ruthenocene 1,2-dicarboxylic acid, carboxylic anhydride, and acid chloride: A facile route to metallocene-fused acenequinones. Organometallics 2011, 30, 3254-3256, doi:10.1021/om2003915.
7. Batterjee, S.M.; Marzouk, M.I.; Aazab, M.E.; El-Hashash, M.A. The electrochemistry of some ferrocene derivatives: redox potential and substituent effects. Applied Organometallic Chemistry 2003, 17, 291-297, doi:org/10.1002/aoc.414.
8. Emília, M.; Silva, N.P.R.A.; Pombeiro, A.J.L.; da Silva, J.J.R.F.; Herrmann, R.; Deus, N.; Castilho, T.J.; Silva, M.F.C.G. Redox potential and substituent effects at ferrocene derivatives. Estimates of Hammett σp and Taft polar σ substituent constants. Journal of Organometallic Chemistry 1991, 421, 75-90, doi:org/10.1016/0022-328X(91)86433-Q.
9. Hoh, G.L.K.; McEwen, W.E.; Kleinberg, J. Substituent Effects in the Chronopotentiometric Oxidation of Ferrocenes. Journal of the American Chemical Society 1961, 83, 3949-3953, doi:10.1021/ja01480a005.
10. Hall, D.W.; Russell, C.D. Substituent effects in the chronopotentiometric oxidation of ferrocene derivatives. Internal solvation of certain substituted ferricenium ions. Journal of the American Chemical Society 1967, 89, 2316-2322, doi:10.1021/ja00986a012.
11. N.P.R.A. Silva, M.E.; Pombeiro, A.J.L.; Fraústo da Silva, J.J.R.; Herrmann, R.; Deus, N.; E.Bozak, R. Redox potential and substituent effects in ferrocene derivatives: II. Journal of Organometallic Chemistry 1994, 480, 81-90, doi:org/10.1016/0022-328X(94)87105-1.
12. Sheldrick, G. SHELXT - Integrated space-group and crystal-structure determination. Acta Crystallographica Section A 2015, 71, 3-8, doi:10.1107/S2053273314026370.
13. Sheldrick, G. Crystal structure refinement with SHELXL. Acta Crystallographica Section C 2015, 71, 3-8, doi:10.1107/S2053229614024218.
14. Patwa, A.N.; Gupta, S.; Gonnade, R.G.; Kumar, V.A.; Bhadbhade, M.M.; Ganesh, K.N. Ferrocene-linked thymine/uracil conjugates: base pairing directed self-assembly and supramolecular packing. Journal of Organic Chemistry 2008, 73, 1508-1515, doi:10.1021/jo7023416.
15. Apreutesei, D.; Lisa, G.; Hurduc, N.; Scutaru, D. Synthesis and un-isotherm kinetic study of some ferrocene acids. Central European Journal of Chemistry 2004, 2, 553-562, doi:org/10.2478/BF02482720.
16. Huffman, J.; Rabb, D. Notes- The Preparation of 1,2-(α-Ketotetramethylene)ferrocene. The Journal of Organic Chemistry 1961, 26, 3588-3589, doi:10.1021/jo01067a653.
17. Rinehart, K.L., Jr.; Curby, R.J., Jr.; Gustafson, D.H.; Harrison, K.G.; Bozak, R.E.; Bublitz, D.E. Organic chemistry of ferrocene. V. Cyclization of ω-ferrocenylaliphatic acids. Journal of the American Chemical Society 1962, 84, 3263, doi:10.1021/ja00876a010.
18. King, R.B.; Bisnette, M.B. π-Cyclopentadienyl-π-indenyliron. Angewandte Chemie International 1963, 75, 642, doi:org/10.1002/anie.196304003.
19. Bernhard, Y.; Gilbert, J.; Bousquet, T.; Favrelle-Huret, A.; Zinck, P.; Pellegrini, S.; Pelinski, L. One-Pot Synthesis of 2,5-Disubstituted Furans through In Situ Formation of Allenes and Enolization Cascade. European Journal of Organic Chemistry 2019, 2019, 7870-7873, doi:10.1002/ejoc.201901669.
20. Liu, G.; He, H.; Wang, J. Ferrocene redox controlled reversible immobilization of ruthenium carbene in ionic liquid: a versatile catalyst for ring-closing metathesis. Advanced Synthesis & Catalysis 2009, 351, 1610-1620, doi:10.1002/adsc.200800713.
21. Weißenbacher, M.; Sturm, T.; Kalchhauser, H.; Kratky, C.; Weissensteiner, W. Synthesis and characterization of novel aminophosphine ligands based on ferrocenodecaline backbones. Monatshefte für Chemie 2002, 133, 991-1009, doi:10.1007/s007060200069.
22. Nesmeyanov, A.N.; Vol'kenau, N.A.; Vil'chevskaya, V.D. Intramolecular acylation in the ferrocene series. Cyclization of γ-ferrocenyl substituted acids and oxo acids. Doklady Akademii Nauk SSSR 1958, 118, 512.
23. Osiecki, J.H.; Hoffman, C.J.; Hollis, D.P. Organometallic compounds. Ruthenium and iron derivatives of indene. Journal of Organometallic Chemistry 1965, 3, 107, doi:10.1016/s0022-328x(00)84739-7.
24. Hanlan, A.J.L.; Ugolick, R.C.; Fulcher, J.G.; Togashi, S.; Bocarsly, A.B.; Gladysz, J.A. Chemistry via metal atom cocondensation: isomerization and complexation reactions of organocyclopropanes and spirocycles. Inorganic Chemistry 1980, 19, 1543-1551, doi:10.1021/ic50208a023.
25. Austin, R.N.; Clark, T.J.; Dickson, T.E.; Killian, C.M.; Nile, T.A.; Schabacker, D.J.; McPhail, A.T. Synthesis and properties of novel substituted 4,5,6,7-tetrahydroindenes and selected metal complexes. Journal of Organometallic Chemistry 1995, 491, 11-18, doi:10.1016/0022-328x(94)05247-9.
26. Fleischer, E.B.; Hawkinson, S.W. The structure of [alpha]-keto-1,5-tetramethyleneferrocene. Acta Crystallographica 1967, 22, 376-381, doi:10.1107/S0365110X67000738.
27. Schlögl, K. Stereochemistry of Metallocenes. In Topics in Stereochemistry; 1967; pp. 39-91.

28. Paramasivam, S.; Purushothaman, S.; Seshadri, P.R.; Raghunathan, R. (E)-1-Ferrocenyl-3-[2-(2-hydroxyethoxy)phenyl]prop-2-en-1-one. Acta Crystallographica Section E 2013, 69, m144, doi:10.1107/S1600536813003395.
29. Zhang, J.; Yan, S.; He, Z.; Xu, L.; Huang, S. 2-Amino-4-(4-chlorophenyl)-6-ferrocenylpyridine-3-carbonitrile. Acta Crystallographica Section E 2008, 64, m730, doi:10.1107/S1600536808008714.
30. Bratych, N.; Hassall, K.; White, J. Redetermination of the structure of diferrocenyl ketone at low temperature. Acta Crystallographica Section E 2003, 59, m33-m35, doi:10.1107/S1600536802022262.
31. Erben, M.; Ruzicka, A.; Vinklarek, J.; Stava, V.; Handlir, K. 1'-Acetylferrocene-1-carbonitrile. Acta Crystallographica Section E 2007, 63, m2145-m2146, doi:10.1107/S1600536807033892.
32. Erben, M.; Vinklarek, J.; Ruzicka, A. Acetylferrocene-2-chloro-1-ferrocenylethanone (1/1). Acta Crystallographica Section E 2011, 67, m1447-m1448, doi:10.1107/S1600536811038244.
33. Cremer, D.t.; Pople, J. General definition of ring puckering coordinates. Journal of the American Chemical Society 1975, 97, 1354-1358, doi:org/10.1021/ja00839a011.
34. Okuda, J.; Albach, R.W.; Herdtweck, E.; Wagner, F.E. Substituent effects in multiply trimethylsilyl-substituted ferrocenes. Molecular structure of 1,1′,2,2′,4,4′-hexakis(trimethylsilyl)ferrocenium tetrafluoroborate. Polyhedron 1991, 10, 1741-1748, doi:org/10.1016/S0277-5387(00)83794-8.
35. Tateaki, O.; Kazuo, O.; Tadashi, F.; Shunsuke, M.; Taeko, I.; Akira, K.; Nobuyuki, T. Electrochemical properties of ferrocenophanes. I. Voltammetric studies on the oxidation of mono-, di-, and tri-bridged ferrocenophanes in acetonitrile. Bulletin of the Chemical Society of Japan 1981, 54, 3723-3726, doi:10.1246/bcsj.54.3723.